JGR Solid Earth

RESEARCH ARTICLE
10.1029/2023JB026817

The Crustal and Uppermost Mantle Vs Structure of the Middle and Lower Reaches of the Yangtze River Metallogenic Belt: Implications for Metallogenic Process

Yongqian Zhang[1,2], Qingtian Lü[1,2], Danian Shi[1,2], Yingjie Yang[3,4], Juan Carlos Afonso[3,5], Yao Xu[1,2], Jiayong Yan[1,2], Xuejing Gong[1,2], and Tao Xu[6]

[1]Chinese Academy of Geological Sciences, Beijing, China, [2]China Deep Exploration Center—SinoProbe Center, China Geological Survey & Chinese Academy of Geological Sciences, Beijing, China, [3]Department of Earth and Space Sciences, Southern University of Science and Technology, Shenzhen, China, [4]Guangdong Provincial Key Laboratory of Geophysical High-resolution Imaging Technology, Southern University of Science and Technology, Shenzhen, China, [5]Faculty of Geo-Information Science and Earth Observation (ITC), University of Twente, Enschede, The Netherlands, [6]State Key Laboratory of Lithospheric Evolution, Institute of Geology and Geophysics, Chinese Academy of Sciences, Beijing, China

Key Points:

- We obtain a fine Vs structure of the crust and uppermost mantle beneath the MLYMB
- We observe velocity features closely related to the metallogenic process of MLYMB
- We propose a three-stage metallogenic process for the origin of the MLYMB

Supporting Information:

Supporting Information may be found in the online version of this article.

Correspondence to:

Q. Lü and Y. Yang,
lqt@cags.ac.cn
yangyj@sustech.edu.cn

Citation:

Zhang, Y., Lü, Q., Shi, D., Yang, Y., Afonso, J. C., Xu, Y., et al. (2023). The crustal and uppermost mantle Vs structure of the middle and lower reaches of the Yangtze River metallogenic belt: Implications for metallogenic process. *Journal of Geophysical Research: Solid Earth*, *128*, e2023JB026817. https://doi.org/10.1029/2023JB026817

Received 4 APR 2023
Accepted 21 JUL 2023

Author Contributions:

Conceptualization: Yongqian Zhang, Qingtian Lü, Danian Shi, Yingjie Yang
Data curation: Danian Shi, Yingjie Yang, Yao Xu, Jiayong Yan
Investigation: Yao Xu, Jiayong Yan
Methodology: Yongqian Zhang, Qingtian Lü, Yingjie Yang
Resources: Danian Shi, Yingjie Yang
Software: Yongqian Zhang, Yingjie Yang
Supervision: Qingtian Lü, Danian Shi
Validation: Yongqian Zhang, Qingtian Lü, Yingjie Yang
Writing – original draft: Yongqian Zhang, Qingtian Lü
Writing – review & editing: Yongqian Zhang, Yingjie Yang, Juan Carlos Afonso, Xuejing Gong, Tao Xu

Abstract The Middle and Lower Reaches of the Yangtze River metallogenic belt (MLYMB) is one of the most important Fe-Cu polymetallic belts in China. However, the mechanism and deep geodynamical process for the formation of this belt are still controversial. Here, we obtain the crustal and the uppermost mantle structures using ambient noise data from a dense seismic profile. A low velocity zone is revealed beneath the Moho of MLYMB, interpreted as the source of the deep mineralization materials. In addition, a low velocity layer (LVL) and a high velocity layer (HVL) are observed in the crust of the southern segment of the profile. The LVL is interpreted as a tectonic detachment layer between the upper and the lower crust, and the HVL is interpreted as the aggregation zone for mineralizing melts or crystallized magma chambers. Based on the observed velocity features, we propose a three-stage model for the formation of ore deposits in MLYMB. Our model suggests that an upwelling of asthenosphere triggered by the delamination of a previously thickened lithosphere leads to the partial melting of upper mantle rocks, which eventually ponders under the Moho. The magma then infiltrates through the ductile lower crust and reaches a depth of ~7–13 km, forming a minerals-enriched magma chamber. Minerals-rich hot fluids originating from the magma chamber continue to move upward along the pre-existent faults and the minerals finally precipitate in dense veinlets when reaching shallow depths, forming the ore deposits in and around the MLYMB.

Plain Language Summary The formation of large-scale mineral deposits is closely related to the lithosphere structure. The Middle and Lower Reaches of the Yangtze River metallogenic belt (MLYMB) is an ideal place to study the mineral system, as it is one of the most important Fe-Cu polymetallic metallogenic belts in Eastern China and contains more than 200 ore deposits. Yet the mechanism and deep geodynamical process for the formation of this belt are still controversial. In this study, we construct a high-resolution seismic model of the crust and the uppermost mantle using ambient noise data from a dense seismic profile. Our result reveals velocity features closely related to the metallogenic process in this region. Based on the observed velocity features, we propose a three-stage model for the formation of the ore deposits in MLYMB, which is of great importance for the development of "mineral system" approaches to the exploration of minerals worldwide.

1. Introduction

The Middle and Lower Reaches of the Yangtze River metallogenic belt (MLYMB), located in eastern China, is one of the most important metallogenic provinces in China (Figure 1). It contains more than 200 Fe-Cu, Mo, Zn, Pb, and other metallic deposits within seven large ore districts (Chang et al., 1991; Sun et al., 2003). Many previous studies have addressed the tectono-magmatic evolution of the MLYMB and associated metallogenic processes (e.g., Chen & Jahn, 1998; Lapierre et al., 1997; Wang et al., 2006; Xu et al., 2002). Thanks to this body of work, general consensus has been reached on the main tectonic settings and the emplacement age of ore-related granites. The main ore deposits in MLYMB are related to the mineralization of Fe and Cu, which was formed between ~145 – ~120 Ma during a period of transition from compressional to extensional tectonics, followed by an extensive intrusion of A-type granitoids (Dong et al., 2011; Zhou et al., 2008). Also, high-K calc-alkaline rocks were discovered in the middle section of MLYMB (Zhou et al., 2008). These high-K calc-alkaline rocks are

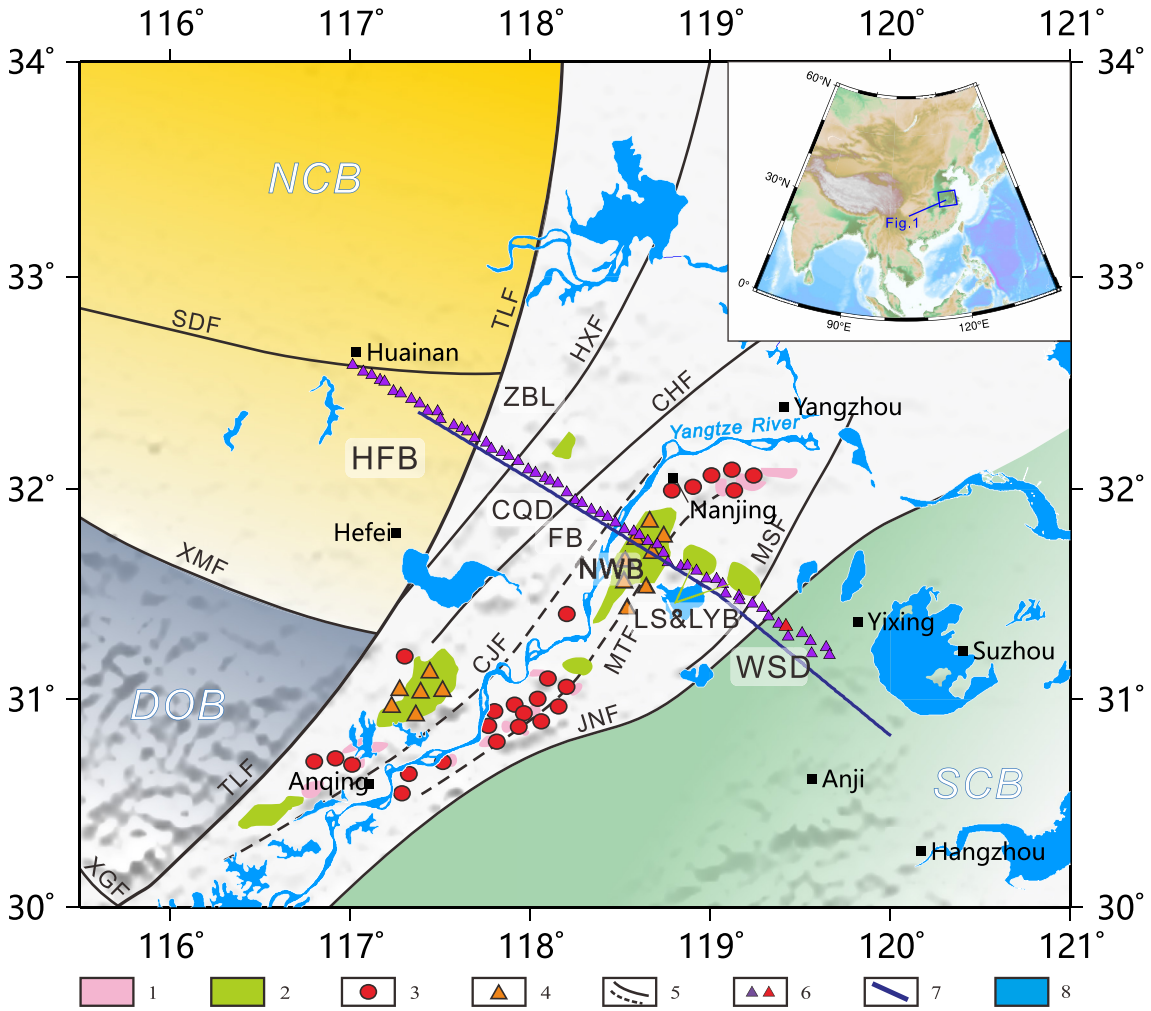

Figure 1. Tectonic framework in and around the Middle-Lower Reaches of Yangtze River metallogenic belt (MLYMB) showing the locations of main ore deposits and the seismic stations used in this study. 1- Late Jurassic- Early Cretaceous granite outcrops (156–137 Ma), 2- Cretaceous volcanics and subvolcanics (<135 Ma), 3- skarn type Fe-Cu or Cu-Au-Mo deposits (>135 Ma), 4- porphyry-type Fe deposits (<135 Ma), 5- faults (dashed line for inferred faults), 6- portable broad-band seismic stations, 7- deep seismic reflection profile (Lü et al., 2015), 8- water area. Abbreviations for the tectonic blocks and faults: NCB- North China Block, SCB- South China Block, DOB- Dabie Orogenic Belt, HFB- Hefei basin, CQD- Chuquan Depression, FB- Chaohu Thrust Fold belt, NWB- Ningwu Basin, LS&LYB- Lishui and Liyang Volcanic Basin, WSD- Wansu Depression; TLF- Tancheng-Lujiang fault, CHF- Chuhe fault, CJF- Changjiang fault, HXF- Huaiyin-Xiangshui fault, MSF- Maoshan fault, MTF- Main thrust fault, JNF- Jiangnan fault (Yangxin-Changzhou fault), SDF- Shouxian-Dingyuan fault, XMF- Xiaotian-Mozitan fault, XGF- Xiangfan-Guangji fault. The red triangle shows the location of station YZ23 and the insert map shows the location of this figure relative to the tectonics of China mainland.

derived from 70% mantle materials and 30% crustal materials (Zhou et al., 2008), and are believed to be closely associated with the mineralization episodes in MLYMB (Lü et al., 2015, 2021; Wang et al., 2006; Xu et al., 2002; Xue et al., 2015). This indicates that deep processes, involving the lithospheric and sublithospheric mantle, played important roles as precursors to mineralization events.

In contrast to the well-characterized mineralization events and shallow tectonics, the nature of the deep geodynamic processes responsible for creating and entraining magma from a deep source and carrying it to shallower emplacement levels remains controversial. Various metallogenic models of ore formation and the associated geodynamic causes have been proposed for this region. They can be categorized into two groups based on the postulated geodynamic scenario. Group 1 contains models that consider the paleo-Pacific subduction and/or its roll-back (e.g., Chen & Jahn, 1998; Lapierre et al., 1997; Li & Li, 2007) as the main geodynamic trigger. Group 2 includes models that are based on the hypothesis that lithosphere delamination and the subsequent asthenospheric upwelling and thermal erosion are the key processes (e.g., Wang et al., 2006; Xu et al., 2002; Xue et al., 2015). As such, these two groups of models predict different footprints on the lithosphere structure and properties

(Hawkesworth et al., 2013; Lü et al., 2013, 2015, 2021). This makes it possible, at least in principle, to map the deep structure of the mineral system and discriminate among the competing models of their formation (Blewett et al., 2010; Griffin et al., 2013; Hawkesworth et al., 2013). This knowledge is important for the application of "mineral system" approaches to the exploration of minerals worldwide (McCuaig et al., 2010).

In 2009–2011, an integrated geophysical probing experiment was carried out along a 330-km long profile across the MLYMB. The aim of this experiment is to study the fine lithosphere structure of the MLYMB and reveal the geodynamic processes and metallogenic background responsible for the formation of polymetallic ore deposits (Lü et al., 2015, 2021). The deep structures along this profile have been studied with various geophysical methods, including deep seismic reflection (Lü et al., 2015, 2021), wide-angle reflection/refraction seismic sounding (Xu et al., 2014), teleseismic receiver functions (Shi et al., 2013) and gravity modeling (Y. Q. Zhang et al., 2014). Among the previous seismic studies, seismic receiver functions and deep reflection are used to constrain interfaces of lithosphere, and wide-angle reflection/refraction is employed to constrain P-wave velocity (Vp) model of the crust. However, no high-resolution S-wave velocity (Vs) model has been constructed along the profile. In general, Vs is more sensitive than Vp to the presence of thermal anomalies, composition changes, partial melts, fluids and shear zones within the lithosphere, which are often related to magmatic and hydrothermal systems (Goes et al., 2000; Jackson & Rigden, 1998). Vs also offers a unique sensitivity to thermal anomalies in the uppermost mantle (Goes et al., 2000; Jackson & Rigden, 1998). Therefore, a high-resolution Vs model can provide critical insights not only into the formation of the ore deposits but also into their root geodynamic causes.

In this study, we collect ambient noise data from seismic stations along a dense linear array and use ambient noise tomography to build a fine Vs model beneath the MLYMB. Our model reveals detailed crustal and uppermost mantle structures that (a) provide constraints on the possible geodynamic settings responsible for the generation of a large-scale magmatic system and (b) indicate how the magma/fluids migrated from the upper mantle to the shallow crust to form discrete ore deposits.

2. Brief Geologic Settings

The MLYMB is located at the boundary between the North China Block (NCB) and the South China Block (SCB) (Figure 1). Structurally, it is surrounded by three regional faults: the Xiangfan-Guangji fault on the southwest, the Tancheng-Lujiang (TLF) on the northwest and the Jiangnan fault (JNF) on the southeast (Figure 1). It also marks the foreland area of the Dabie-Sulu belt and the northeast part of the Yangtze Craton. The regional stratigraphic sequence in the MLYMB contains mainly marine-phase clastic and carbonate rocks deposited on the top of a Precambrian basement during the Cambrian-Triassic (Lower and Middle Devonian strata are absent due to uplift and erosion). Subordinated terrigenous clastic and volcanic units were emplaced in some volcanic basins (e.g., the Ningwu basin) of the MLYMB since the middle Jurassic. This sedimentary sequence was intruded by the Yanshanian A-type granitoids and subvolcanic complexes in the late Mesozoic (Chang et al., 1991; Lü et al., 2013, 2015, 2021; Shi et al., 2013).

According to previous geological studies (e.g., Dong et al., 2011; Li, 1994; Li & Li, 2007; Wu et al., 2000; Yin & Nie, 1993; Zhou et al., 2008), the MLYMB area experienced two orogenies since the Mesozoic: the Indosinian orogeny (~ Early to Middle Triassic) and the Yanshanian orogeny (~ Middle to Late Jurassic). The NCB-SCB collision marks the major event during the Indosinian orogeny, which caused the formation of the TLF and also the ultra-pressure metamorphism in the Dabie Mountains (Li, 1994; Li & Li, 2007; Yin & Nie, 1993). The Yanshanian orogeny was dominated by intra-continental contraction under the effect of the paleo-Pacific plate subduction, which caused widespread uplift and erosion of the eastern part of China mainland (Dong et al., 2011; Wu et al., 2000). The magmatism and metallogenesis in MLYMB occurred mainly in the period between ~145 – ~120 Ma, with a peak in activity between ~135 and ~127 Ma at the Ningwu Basin (Zhou et al., 2008). It is generally believed that this magmatism and the associated mineralization events were a consequence of a compression-to-extension tectonic regime shift during the post-orogeny stages in the Early Cretaceous (Chang et al., 1991; Dong et al., 2011; Zhou et al., 2008).

Since the period of the late Cretaceous, the tectonics in and around the MLYMB has been in a stable or weak extensional environment. Magmatism has been limited to some local areas and Late Cretaceous red beds were deposited in the extensional basins. The relatively stable tectonic environment facilitates the reservations of ancient tectonic structures formed before the Late Cretaceous, making it possible to infer the past geodynamics by investigating the present crustal structures beneath the MLYMB.

The seismic profile analyzed in this study trends in the NW-SE direction and is nearly perpendicular to all major tectonic discontinuities, including the large TLF that separates the NCB and the SCB. The profile runs across five

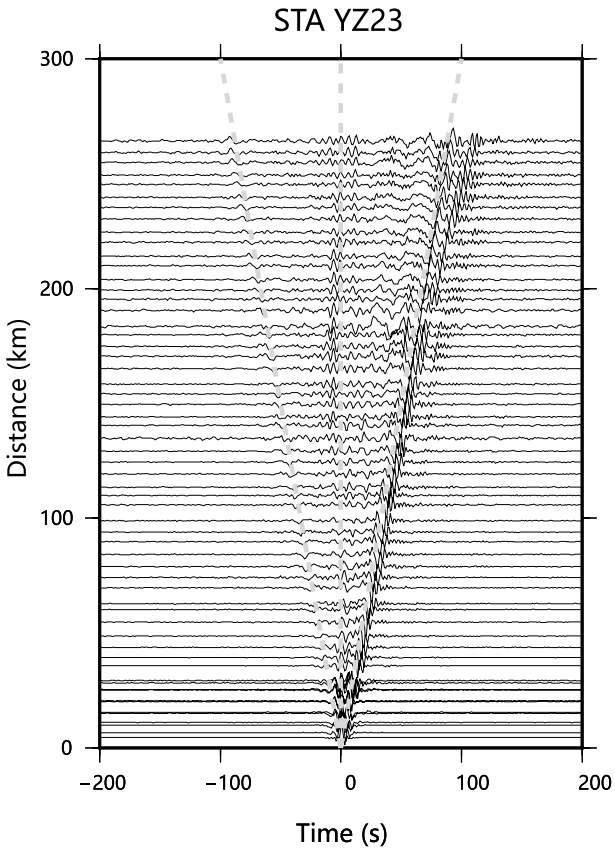

Figure 2. Stacked cross-correlation record section of station YZ23 with other stations, and the location of YZ23 is shown as a red triangle in Figure 1.

tectonic sub-units, including (from northwest to southwest) the Hefei basin (HFB), the Zhangbaling uplift (ZBL), the Chuquan depression (CQD), the MLYMB, and the Wansu depression (WSD). These units are separated by the TLF, the Huaiyin-Xiangshui fault, the Chuhe fault, and the JNF. Furthermore, the MLYMB contains three additional sub-units: the Chaohu fold-thrust belt, the Ningwu volcanic basin (NWB), and the Lishui and Liyang volcanic basin (LS&LYB) (Figure 1).

3. Data and Method

3.1. Data Acquisition

We collect continuous seismic noise data from a 300-km long linear array traversing the Anhui and Zhejiang provinces (Figure 1; Table S1 in Supporting Information S1). This array was deployed during a period from November 2009 to August 2011 with a total of 60 broadband seismic stations. The average station spacing is about 5 km. All stations are equipped with Guralp CMG-3ESPCD seismometers with a bandwidth of 0.02–60 s. The sampling rate of the seismic records is 100 sample-per-second (sps). The close station spacing allows us to characterize the fine crustal Vs structure of the MLYMB with unprecedented resolution.

3.2. Data Processing Procedures

3.2.1. Cross-Correlations

We follow the flow chart suggested by Bensen et al. (2007) and Yang et al. (2007, 2008) to extract surface waves from cross-correlations of continuous seismic records. Our data processing steps are as follows: (a) cut raw continuous seismic noise data to a series of 1-day records, and then decimate the sampling rate of the time series from 100 sps to 1 sps; (b) remove the instrument responses from the continuous data and apply band-pass filtering of 5–150 s to continuous data; (c) apply a running average normalization method to the filtered data to remove the effects of strong noise sources (such as earthquakes), and whiten each record in spectral domain to avoid significant spectral imbalance (Guo et al., 2016; Yang et al., 2007, 2008; Yao et al., 2006); (d) cross-correlate the processed daily time series between all pairs of the 60 stations. Finally, we stack all the daily cross-correlations over the deployment duration of the seismic array to obtain the stacked cross-correlation functions (CCFs).

Examples of the stacked CCF of station YZ23 with other stations are shown in Figure 2. We notice that the amplitudes of the causal (positive lag part) and acausal (negative lag part) lags of the CCFs are asymmetric with much stronger signals appearing in the positive lag. This is because our seismic profile trends in the NW-SE direction and the ambient noise sources coming from the coast in the southeast are much stronger than those from the continent in the northwest. We thus stack the positive and negative lags of each CCF to form the symmetric component, and all subsequent data analyses are performed on symmetric components.

3.2.2. Dispersion Measurements

After obtaining all the interstation CCFs, we measure dispersion curves of Rayleigh wave phase velocities at 5–30 s by utilizing an automatic frequency-time analysis method (FTAN) (Levshin & Ritzwoller, 2001). To get reliable dispersion data for tomography, we employ three criteria to control the quality of data: (a) signal-to-noise ratios (SNRs) of CCFs need to be >10; (b) the interstation distances of CCFs need to be >1.5 wavelengths of Rayleigh waves, as Luo et al. (2015) indicate dispersion measurements from CCFs with short interstation distances up to only one wavelength are still reliable for tomography; (c) dispersion curves should be coherent with each other, and outliers of dispersion curves with deviations more than 10% from the mean values are discarded. After applying these criteria, we retain a total of 1,172 dispersion curves for the subsequent surface wave tomography. The average of all dispersion curves of Rayleigh wave phase velocity along with their standard

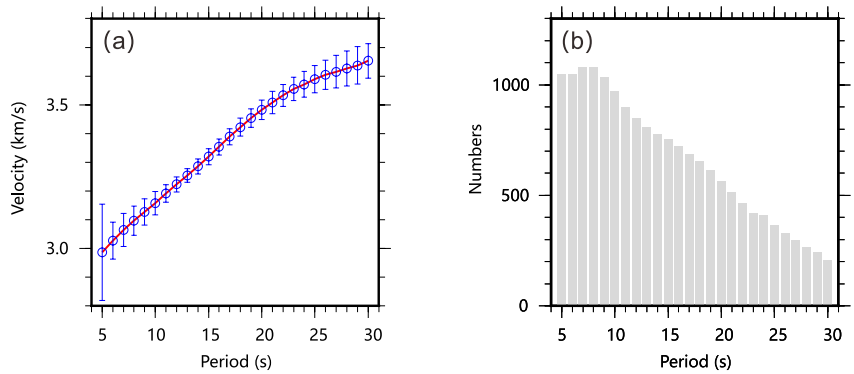

Figure 3. (a) Averaged phase velocity dispersion curve of all the possible station-pairs of our stations crossing MLYMB, and the vertical bars represent the standard deviation at each period; (b) Numbers of the dispersion data at each period.

deviations and the number of the dispersion data at each period are plotted in Figures 3a and 3b. The number of phase velocity measurements decreases with increasing periods.

3.2.3. Rayleigh-Wave Phase Velocity Tomography

We obtain 2-D Rayleigh wave phase velocity maps at individual periods by employing the Fast Marching Surface-wave Tomography (FMST) method developed by Rawlinson and Sambridge (2005). In the implementation of FMST, we parameterize our study area of a corridor along the seismic array using a $0.1° \times 0.1°$grid (Figure S1 in Supporting Information S1). Damping (ε) and smoothing (η) are required in the FMST. The damping term controls the variations of amplitude of velocity anomalies and the smoothing term dictates the roughness of lateral velocity variations. We determine the optimal values of the two parameters via examining the trade-off curves between data misfits and model roughness after tests using various combinations of these two parameters (Figure S2 in Supporting Information S1).

Here, we are mainly interested in lateral variations of phase velocities along the linear seismic array. Thus, we plot phase velocity variations along the profile as a 2-D map in Figure 4a by assembling 5–30 s periods phase velocity profiles. Relative phase velocity perturbations at each period are also plotted in Figure 4b. In this figure (and also in Figure 4a, albeit less clear), differences in phase velocities on the north and south segments are evident. In the NCB, low phase velocities dominate at short periods (5–15 s) whereas high phase velocities dominate at long periods (>15 s). The middle portion of the profile (east from the TLF) exhibits a large low phase velocity anomaly at periods longer than 17 s and a fast anomaly at shorter periods. Toward the southern segment of the profile, low phase velocities could be identified at short and intermediate periods.

3.2.4. Shear-Wave Velocity (Vs) Inversion

We extract local Rayleigh wave dispersion curves at each grid point from the 2-D phase velocity image presented in Figure 4. Then, we employ a Bayesian inference approach developed by Afonso et al. (2013) to invert each grid-node Rayleigh wave dispersion curve for a 1-D Vs column along the profile. In the Bayesian approach, a posterior probability density function (PDF) is constructed to represent the solution of the inverse problem. Since this PDF has no analytical expression in the present context, we generate an approximation of the PDF via a Markov-chain Monte-Carlo (MCMC) sampling algorithm. Details on the inversion approach can be found in Afonso et al. (2013) and Guo et al. (2016).

In the inversion, model parameterization and prior information are detailed as follows: (a) the maximum inversion depth is set to 100 km as the longest period of our dispersion data only reaches 30 s, which has the highest sensitivity to Vs at depths shallower than ~100 km; (b) a sedimentary layer is included in the uppermost crust; its thickness is allowed to vary between 0 and 8 km; its velocity is set to vary between 1.2 and 2.5 km/s at the surface and between 1.5 and 3.5 km/s at the bottom; (c) the depth of the Moho is set initially based on the results of receiver functions (Shi et al., 2013) and is allowed to vary within a range of ±5 km and seismic velocity is forced to increase across the Moho; (d) the initial 1-D velocity model is set based on a 3-D reference model of Shen et al. (2016) and two sets of four B-spline functions are adopted to describe the 1-D Vs in the crust and the upper mantle, respectively. The variation range of Vs is set to be within ±20% of the initial model for all layers

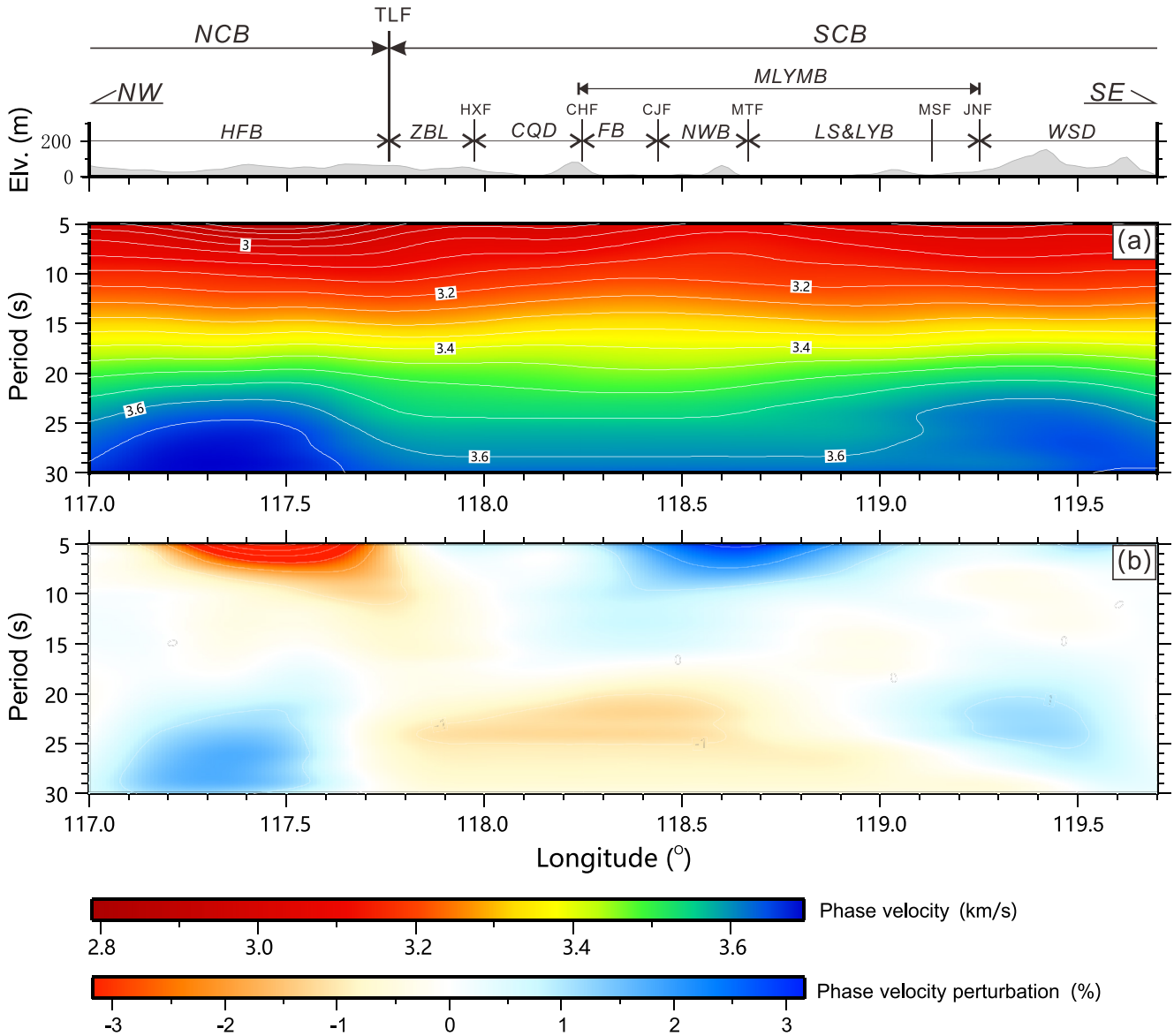

Figure 4. Absolute (a) and relative (b) phase velocities of Rayleigh wave phase velocities along the seismic profile, with topography and main tectonics on the upper panel, and abbreviations for the faults and tectonic units are the same as those in Figure 1.

other than the first sedimentary layer. At each iteration of the MCMC algorithm (i.e., for each sample of the model space), phase velocity dispersions are computed using the code of MINEOS (Masters et al., 2007). After a total number of 150,000 samples, we use the means of respective posteriors of the last 3,000 accepted models in the chain to approximately represent the final results. This is justified as the chain converges quickly and mixes well in this problem (Afonso et al., 2013; Guo et al., 2016; Yang et al., 2021). An example of a 1-D Vs column obtained after the inversion is shown in Figure 5a, demonstrating that surface wave dispersion data are fitted very well by predicted ones calculated from the resulting models.

4. Vs Transects Along the Profile

After inverting local Rayleigh wave dispersion curves for 1-D Vs structure at all grid nodes along the seismic array, we produce a 2-D Vs model by assembling all the 1-D Vs columns (Figure 6a). For comparison, we also superimpose the CCP stack of P wave receiver functions (Shi et al., 2013) on our Vs model in Figure 6b, which shows strong converted phases from the Moho, approximately matching the depths of the strongest vertical Vs gradients of our model.

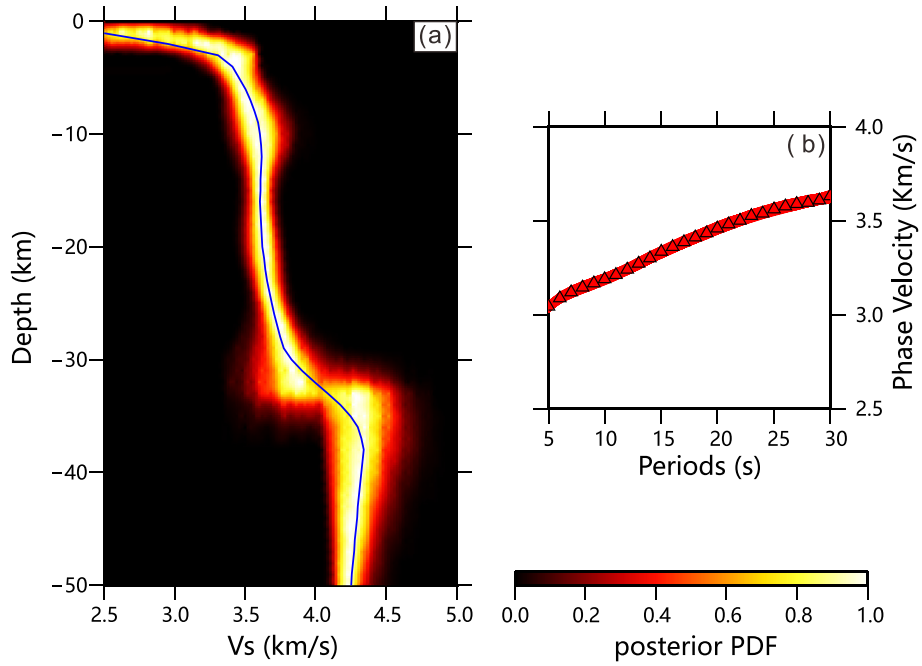

Figure 5. Example of the inversion process of the Markov-chain Monte-Carlo scheme at the grid point of 118.47E, 31,81N (near the Yangtze River) (a) inversed 1-D S-wave velocity column at the grid point, the color scale on the right side represents the normalized posterior probability density function and hot zones in (a) denote a higher possibility of the Vs distributions, and the blue line is the average model from posterior PDF; (b) Phase velocity dispersion curves, black triangles are from the ambient noise tomography, and red lines are the last 3,000 accepted models predicated from the 1-D S-wave model of (a).

Beneath the NCB (or HFB, more specifically), the crust can be characterized by a two-layered model according to the Vs structure: a low-velocity sedimentary layer and a high-velocity crystalline crustal layer. Vs increases from ∼2.8 km/s on the surface to ∼3.4 km/s at the bottom of the sedimentary layer, and then from ∼3.4 km/s to 3.8–3.9 km/s near the Moho. The Vs increase imaged beneath the NCB is a typical feature of an old and cold cratonic crust (Allmendinger et al., 1987; Rudnick & Fountain, 1995).

The Vs structure changes abruptly to the east of the TLF, exhibiting more complex patterns beneath the SCB than that beneath the NCB (Figure 6a). In the segments crossing the ZBL and the CQD, Vs increases gradually with depth and toward the southeast. A low-velocity upper crust with a thickness of about 15–20 km and a high-velocity lower crust with a thickness of about 10–15 km constitute this portion of the profile. In the MLYMB segment, the crust is characterized by a low-Vs layer (LVL) and a high-Vs layer (HVL) beneath the NWB and the LS&LYB sub-units. The mid-crust LVL is located at a depth of ∼13–20 km, and it is also noticeable in a profile sub-parallel to ours but ∼150 km southwest (Li et al., 2020). As for the HVL, it is located at a depth of ∼7–13 km with a thickness of ∼6 km, and its velocities are comparable to those imaged at similar depths beneath the NCB. This HVL was also observed in an early 3-D ANT study (Luo et al., 2019) and a P-wave velocity model derived from local seismic tomography (Chen et al., 2020) in this area, but their location and size were not well constrained due to the lower resolution of those studies (∼0.5–1° resolution). In the uppermost mantle, a conspicuous dome-shaped low-Vs zone (LVZ) is imaged with its center located under the CJF (corresponding to the Yangtze River) in the central part of the profile.

5. Discussion

5.1. LVZ Beneath the Moho

One of the most striking features of our Vs model is a LVZ right beneath the Moho at the center of our profile (Figure 6). LVZs in the upper mantle of this region were also imaged in previous studies, albeit with lower resolution. For instance, regional seismic studies identified LVZs at a depth range of 40–140 km beneath the MLYMB (Li et al., 2018; Ouyang et al., 2014). Teleseismic P-wave receiver functions (Shi et al., 2013; Y. Q. Zhang

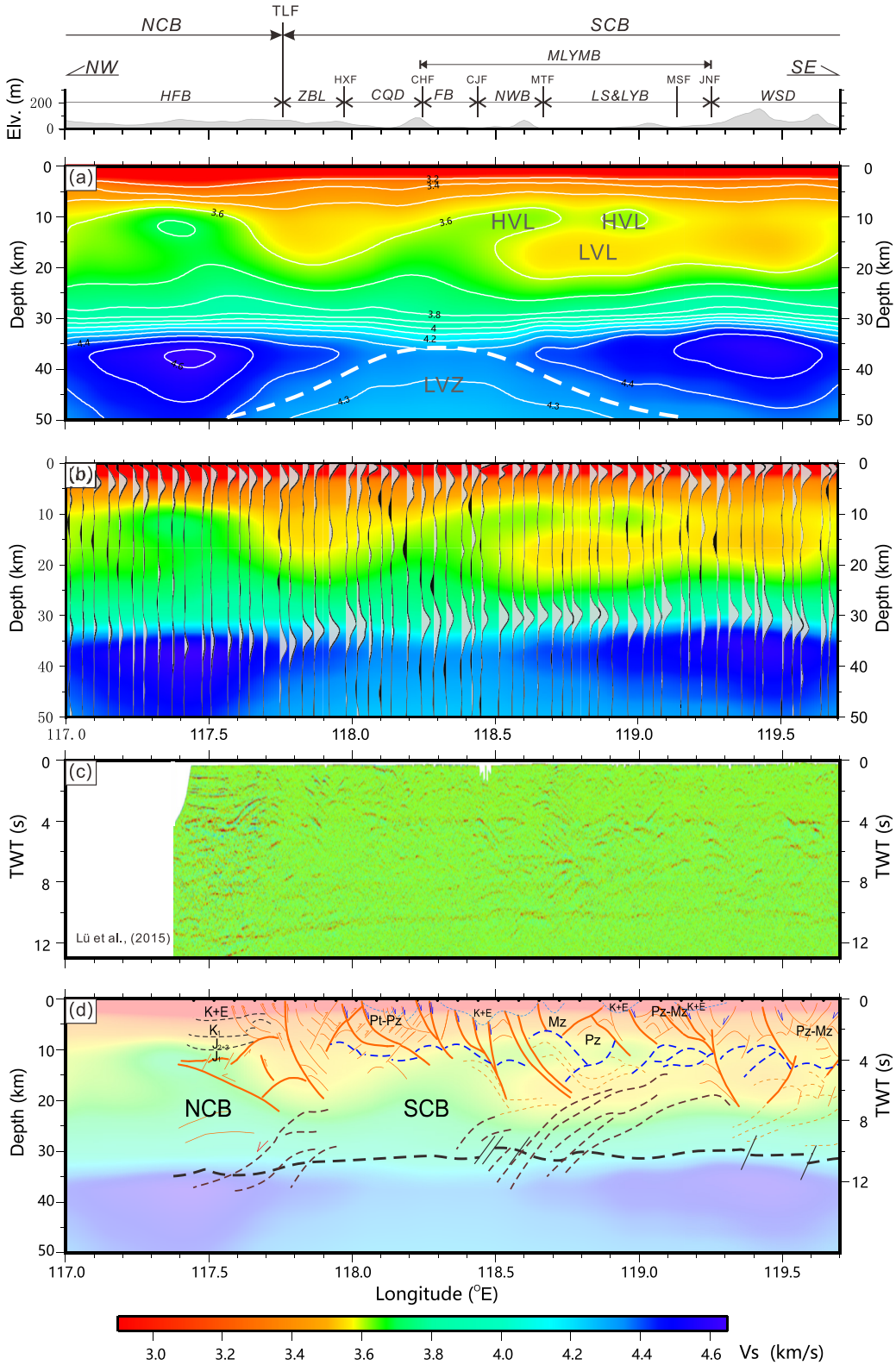

Figure 6.

et al., 2021) and gravity studies (Yan et al., 2021; Y. Q. Zhang et al., 2014) suggested a Moho uplift and a thin lithosphere beneath the MLYMB, suggestive of hot and low velocity materials in the lithospheric mantle. This LVZ may extend downward to depths of about 100–200 km, as suggested by studies from P-wave tomography (Jiang et al., 2014) and S-wave tomography (e.g., Li et al., 2018; Ouyang et al., 2014; Xu et al., 2015) based on teleseismic events. Our dense seismic array and good quality data allow us to map the uppermost shape of this LVZ with higher resolution and confidence than previous works, offering solid ground-truthing for genetic interpretations.

Given the magnitude of the velocity anomaly in the LVZ, its origin is likely associated with thermal anomalies and the presence of hydrated minerals as a result of fluid and magma migration from the upper mantle (e.g., Goes et al., 2000; Jackson and Rigden, 1988; Richards, 2003). Two recent upper mantle thermochemical studies in South China based on multi-observable probabilistic inversion revealed localized temperatures of ~800°C at a depth of 40 km beneath the MLYMB (Yang et al., 2021; A. Zhang et al., 2020), also suggesting a thermal origin for this LVZ. All these observations are consistent with a thin lithosphere beneath the MLYMB.

As mentioned in the introduction, geodynamic models proposed for this region can be classified into two groups. One favors the paleo-Pacific plate subduction as the main geodynamic scenario (active margin) for the Jurassic-Cretaceous tecto-magmatic activity and related mineralization events (e.g., Chen & Jahn, 1998; Lapierre et al., 1997; Li & Li, 2007); the other advocates lithosphere delamination and associated intracontinental extension (e.g., Wang et al., 2006; Xu et al., 2002; Xue et al., 2015). Combining the observation of the LVZ shape with other observations, we notice a number of features as discussed below that favor delamination as the main driving force for the origin of the MLYMB.

The LVZ is localized only beneath the MLYMB and its top reaches the depths of Moho at ~35 km (Figure 6a). Similarly, receiver function studies (Shi et al., 2013; Y. Q. Zhang et al., 2021) revealed a thin crust (~30 km) and a faint LAB in this region. Therefore, both studies indicate there is no significant upper mantle lithosphere existing beneath MLYMB, suggesting that the upper mantle lithosphere of MLYMB has been nearly completely removed. Although the geodynamic processes related to subduction could cause lithosphere thinning, subduction-induced lithospheric thinning is generally widespread and the extent of lithosphere thinning is usually limited to the lower part of lithosphere, not completely removing the whole upper mantle lithosphere. Therefore, we consider delamination is the main mechanism that removes most of the upper mantle part of the lithosphere along with the lowest part of the crust.

In addition, the localized strong thermal disturbance caused by the upwelling of asthenosphere right after the delamination of the thickened lithosphere could trigger partial melting of the lower crustal materials. The melt from the lower crust could mix with the melt originating from the partial melting of upwelling asthenosphere. Indeed, studies of shoshonites (Xue et al., 2015) and adakite-like rocks (Wang et al., 2006; Xu et al., 2002) suggest that the magma in MLYMB was intrinsically formed by the thickened mafic lower crustal partial melting (>40 km) with involvement of mantle component. These studies indicate that there exist crustal-mantle materials mixing and removal of the lower crust below the MLYMB, further supporting the delamination model.

Lithosphere delamination in the MLYMB is thought to occur in response to a sequence of post-orogenic extension events following the NCB-SCB collision (e.g., Dong et al., 2011; Gao et al., 1999; Hu et al., 2020). The continental collision first caused strong compression and led to the formation of the Qinling-Dabie orogen and the thickening and densifying of the lithosphere (e.g., Mattauer et al., 1985; Xu et al., 2002; Yin & Nie, 1993). In the post-orogenic period, delamination occurred along with the geodynamic environment changing from compression to extension. The resultant forced upwelling of asthenospheric mantle provides additional heat and shallow melting, enhancing lithospheric erosion and weakening, which could in turn lead to further delamination (Kay & Kay, 1993; Lü et al., 2015, 2021; Wang et al., 2006; Xue et al., 2015).

5.2. Intra-Crustal Velocity Anomalies Beneath the MLYMB

The NCB is characterized by a typical cratonic crust, with Vs gradually increasing with depth and displaying small lateral velocity variations (Figure 6a). This is in marked contrast with the complex velocity structure of the

Figure 6. Comparison of passive- and active-source seismic observations, with the upper panel showing the topography and the main tectonics along this profile. (a) The 2-D shear-wave velocity model obtained in this study, where the high velocity layer indicates the intra-crustal high-Vs layers, the low velocity layer indicates the intra-crustal low-Vs velocity layer, and the low velocity zone indicates the low-Vs zone in the lithospheric mantle; (b) CCP stacks of P-wave receiver functions (Shi et al., 2013) superimposed on the Vs model derived in this study; (c) Pre-stack time migration imaging of active-source deep seismic reflection profile (Lü et al., 2015); (d) Stacked map of the S-wave velocity model(transparent) derived in this study and the structural lines derived from (c) (Lü et al., 2015).

adjacent SCB. The most prominent feature of the MLYMB intra-crustal structure is a LVL with a depth range of 13–20 km, which we interpret as a part of a trans-crustal shear zone. To investigate the properties and origin of this LVL, we compare our result with a co-line, high-resolution deep reflection seismic imaging (Figure 6c) (Lü et al., 2015, 2021) by superimposing the interpreted structures in the reflection section on our 2-D Vs model (Figure 6d). We find that the LVL in our model correlates well with the location of the "decoupling zone" imaged in the deep seismic reflection section (Lü et al., 2015). Similar LVLs have been observed within the crust of other orogenic belts, such as the eastern Alps and the Canadian Cordillera (Hsü, 1979; Oxburgh, 1972; Price, 1986), and are revealed as good reflectors in deep seismic reflection records (Jones & Nur, 1984; Lü et al., 2015, 2021). They usually mark a mechanical weak zone (brittle-ductile transition), leading to the detachment between the upper and lower crust (Dong et al., 2011; Jones & Nur, 1984; Li, 1994; Oxburgh, 1972).

Continental collision in orogenic processes could contribute to the development of such tectonics of detachment (Doin & Henry, 2001; Li, 1994; Oxburgh, 1972). Along with the convergence between two tectonic blocks, the low-density upper crust deforms as nappe tectonics or thrust-related folds above the detachment layer, while the high-density lower crust underthrusts and forms a crustal "crocodile" structure or flake tectonics (Li, 1994; Lü et al., 2015, 2021; Meissner, 1989; Oxburgh, 1972). The crocodile or flake tectonics refers to the specific clearly diverging and rather plane, strong, reflectors, often observed in the middle and lower crust in the seismic migrated sections (Meissner, 1989; Oxburgh, 1972). This kind of tectonics usually implies a compression environment at its generation time. Specific to the MLYMB, we infer that the detachment may originally be formed in the NCB-SCB collision during the Indosinian orogeny, and later exposed in the metamorphic core complexes near Lushan (Dong et al., 2011; Li, 1994; Yin & Nie, 1993). During the Yanshanian orogeny, the detachment belt was reactivated as a shear zone and strengthened the decoupling between the upper and lower crust.

As for the HVL observed at depths of ~7–13 km in our Vs image (Figure 6a), we prefer to interpret it as a crystallized magma chamber, which is consistent with the interpretation of ore-related magma intrusion documented by Luo et al. (2019) and Chen et al. (2020). Previous studies have shown that the HVL beneath the ore concentration district is generally related to the intrusive rocks and corresponds well with the outcrops of mineral deposits (Flóvenz & Gunnarsson, 1991). Various geologic and isotopic studies suggested that 5–15 km is a normal depth of a magma chamber wherein porphyry deposits originate (e.g., Hedenquist & Lowenstern, 1994; Plank et al., 2013). By thermal modeling and statistical simulations of the genesis of porphyry deposits, Chelle-Michou et al. (2017) suggested that this depth could provide an ideal environment for the cooling, crystallizing, and degassing granitic pluton, and thus may be an important control on the endowment of the giant deposits. Therefore, we tend to interpret the HVL as a remnant paleo-magma-chamber which have cooled and crystallized after intruding to this depth in the Early Cretaceous. Enriched magma ascended from mantle sources triggered by the delamination of SCLM propagated upwards and reached a rheological barrier ponding near the detachment shear zone. At this depth, the large volume of magma body degassed and fed sufficient metalliferous fluids for the ore deposits at shallow depths.

5.3. Implications for the Geodynamics and Metallogenic Processes

Large or super-large metallogenic backgrounds are characterized by fluid/melt systems originating from the deep crust and upper mantle. To better understand the processes that lead to the formation of ore deposits, Wyborn et al. (1994) proposed the concept of "mineral system" and defined it as all geological factors and processes controlling the creation, formation and deposition of mineral deposits. A whole mineral system is linked with knowledge of the geodynamic setting combined with information regarding the crustal/lithospheric architecture, the location of fluid pathways and inferred magmatic bodies. In the context of this work, we aim to reveal the main components and processes defining a "mineral system" in the MLYMB by using high-resolution seismic imaging.

As previously mentioned, the tectonic environment of MLYMB has been generally stable or in weak extension since the Late Cretaceous. This allows us to study the deep fossil structures and the related magmatism and metallogenesis formed before the Late Cretaceous. Specifically, by combining the Vs model obtained in this study with information from previous geological, geochemical and geophysical studies, we infer the geodynamical background and the magma/fluid pathways in the MLYMB as follows by summarizing all the preceding discussions.

Overall, the tectonic movements and crustal deformation during the periods of Indosinian orogeny (~ Early to Middle Triassic) and Yanshanian orogeny (~ Middle to Late Jurassic) created the necessary structures for the

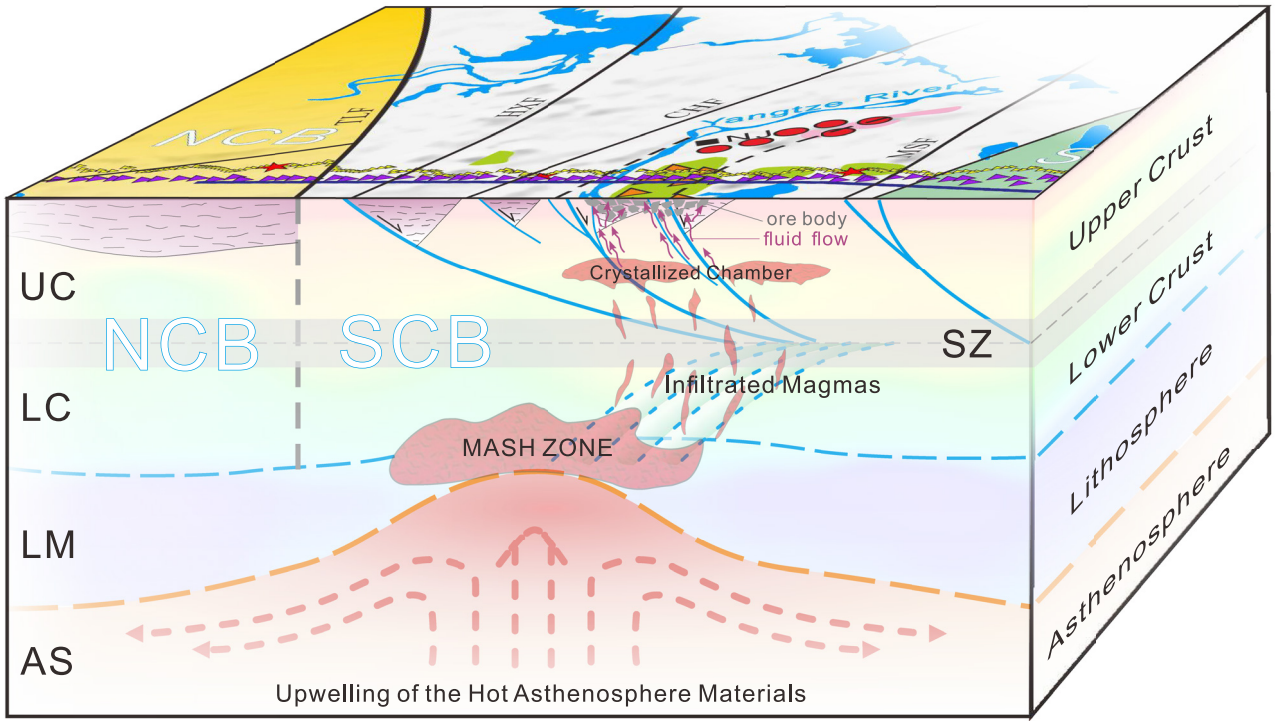

Figure 7. Cartoon model illustrating the three-stage metallogenic process beneath the MLYMB. Abbreviations are as follows: NCB- North China Block, SCB- South China Block, UC- Upper crust, LC- Lower crust, LM- Lithospheric mantle, AS- asthenosphere, SZ- Shear zone, MASH- Melt, Assimilation, Storage and Homogeneous metallogenic process. The near-horizontal dashed blue line marks the Moho discontinuity, the dashed orange line indicates the lithosphere-asthenosphere boundary (LAB), the blue lines in the crust mark the deep faults in the upper crust, and underthrust movement traces (dashed blue line) of the lower crust.

generation and transportation of metalliferous magmas, and the formation and preservation of mineral deposits. The Indosinian orogeny produced the detachment shear zone between the upper and lower crust (Dong et al., 2011; Lü et al., 2015, 2021). During the Yanshanian orogeny, the lower crust of the SCB further decoupled with the overlying upper crust along the pre-formed shear zone, and underthrusted northwestward to the depth (Lü et al., 2015, 2021). The continuous compression and underthrusting thickened the crust and lithosphere beneath the MLYMB, and the thickened lower crust began to get eclogitized when reaching depths >40 km (Kay & Kay, 1993; Price, 1986). Subsequently, the eclogitized lower crust and part of the underlying lithosphere mantle collapsed and delaminated into the asthenosphere during the post-orogenic period (~ Late Jurassic to Early Cretaceous). The delamination eventually caused asthenosphere upwelling to fill the void left by the delaminated part.

As for the metallogenic process, we suggest that a three-stage model can depict the mineral system in the MLYMB (Figure 7), based on the above structures and evidence. This model is updated from the multi-level magma chamber system (Hou et al., 2017; Lü et al., 2013, 2021; Richards, 2003; Vigneresse, 1995), and it specifically contains three stages for the generation, transportation of the metalliferous magmas and formation of the metal-mineral deposits.

First, asthenosphere materials in the upwelling forced by the delamination process began to partially melt when reaching shallow depths. The melt ascended and then ponded at the base of the crust, a mechanism known as crustal underplating (Cox, 1980; Furlong & Fountain, 1986; Thybo & Artemieva, 2013). The heat released by the upwelling material could also lead to the partial melting of any remaining lithosphere, forming a MASH (Melting, Assimilation, Storage, Homogeneous) zone beneath the MLYMB (Hildreth & Moorbath, 1988; Richards, 2003; Lü et al., 2013, 2021; Shi et al., 2013). This MASH zone is exhibited as the LVZ in our seismic imaging and probably acted as the first-stage magma/fluid concentration of the mineral system in the MLYMB.

Later, the partially melted crystallizing magmas infiltrated through the ductile lower crust and released volatiles during their decompression. Pre-existing shear zones facilitated the magma ascent to depths of ~10 km, indicated

by the HVL in the seismic imaging (after full crystallization). This depth is also a place where the degassing magma bodies are emplaced (Hedenquist & Lowenstern, 1994; Plank et al., 2013), and is essential for forming the overlying ore deposits (Chelle-Michou et al., 2017). This HVL marks the second-stage magma/fluid concentration of the mineral system in the MLYMB.

Subsequently, the mineral-rich hot fluids from the magma body at ~7–13 km depths move up along dense veinlets associated with various normal faults existing in the brittle upper crust. When reaching shallow depths of the crust, the temperature and pressure of mineral-rich fluids drop, and minerals begin to precipitate from the mineral-rich fluid. These processes continue to operate for a long period of time to make up the ore deposits we observe at surface or shallow depths. This is the third-stage magma/fluid concentration of the mineral system in the MLYMB. Beneath the NWB, the pre-existing normal faults including CJF, MSF and many small-scale veinlet-like faults among them play an important role as the upward migration channels for the mineral materials. In contrast, although the LS&LYB are located in the same tectonic background within NWB, its lack of ore deposits may be due to the fact that normal faults in this area are not well developed.

6. Conclusions

We image fine crustal S-wave velocity structures along a dense broadband seismic profile crossing the Middle and Lower Reaches of the Yangtze River Metallogenic Belt (MLYMB). Our results reveal distinct crustal structures between the NCB and the SCB, with the crust of the NCB displaying typical cratonic features and that of the SCB showing a significantly more complex structure. Based on the Vs structure and other geological information, we propose a three-stage metallogenic model. A pronounced low-velocity zone is observed beneath the Moho and interpreted as the remnants of an original MASH (Melting-Assimilation-Storage-Homogeneous) zone. A low-velocity layer imaged at a depth of ~20 km is interpreted as a shear zone between the upper and lower crust that provided a pathway for the ascent of magma from the MASH zone. A high-velocity layer is revealed at a depth of ~7–13 km and interpreted as a paleo-magma chamber, acting as the direct source for the ore deposits in the shallow crust. In the shallow upper crust, dense veinlets along various normal faults act as the main channels for the upward movement of mineralizing fluids, which control the final formation of the ore deposits in and around the MLYMB.

Data Availability Statement

Datasets for this research are available at https://doi.org/10.6084/m9.figshare.22297906.v1 (Y. Q. Zhang et al., 2023). The data set includes all the cross-correlation functions between all station pairs used as data to construct our velocity model and the resulting shear wave velocity model of this study.

Acknowledgments
The authors sincerely thank many people for their contribution to this work, especially to the technical personnel who participated in the fieldwork. This study is financially supported by the National Natural Science Foundation of China (Nos. 42074099, 42074069 and 41574082), National Key Research and Development Program of China (No. 2016YFC0600201), and the China Geological Survey Project (Nos. DD20221643 and DD20190012). We would like to express our sincere appreciation and deep-felt memory to our good friend, Prof.Zhongjie Zhang, who suddenly passed away 10 years ago (6 September 2013).

References

Afonso, J. C., Fullea, J., Griffin, W. L., Yang, Y., Jones, A. G., Connolly, J. A. D., & O'Reilly, S. Y. (2013). 3-D multiobservable probabilistic inversion for the compositional and thermal structure of the lithosphere and upper mantle. I: A priori petrological information and geophysical observables. *Journal of Geophysical Research: Solid Earth*, *118*(5), 2586–2617. https://doi.org/10.1002/jgrb.50124

Allmendinger, R. W., Nelson, K. D., Potter, C. J., Barazang, M., Brown, L. D., & Oliver, J. E. (1987). Deep seismic reflection characteristics of the continental crust. *Geology*, *15*(4), 304–310. https://doi.org/10.1130/0091-7613(1987)15<304:dsrcot>2.0.co;2

Bensen, G. D., Ritzwoller, M. H., Barmin, M. P., Levshin, A. L., Lin, F., Moschetti, M. P., et al. (2007). Processing seismic ambient noise data to obtain reliable broad-band surface wave dispersion measurements. *Geophysical Journal International*, *169*(3), 1239–1260. https://doi.org/10.1111/j.1365-246x.2007.03374.x

Blewett, R. S., Henson, P. A., Roy, I. G., Champion, D. C., & Cassidy, K. F. (2010). Scale-integrated architecture of a world-class gold mineral system: The Archaean eastern Yilgarn Craton, Western Australia. *Precambrian Research*, *183*(2), 230–250. https://doi.org/10.1016/j.precamres.2010.06.004

Chang, Y. F., Liu, X. P., & Wu, Y. X. (1991). *Copper and iron mineralization belt of middle and lower Yangtze River* (pp. 1–379). Geological Publishing House. (in Chinese).

Chelle-Michou, C., Rottier, B., Caricchi, L., & Simpson, G. (2017). Tempo of magma degassing and the genesis of porphyry copper deposits. *Science Report*, *7*(1), 40566. https://doi.org/10.1038/srep40566

Chen, A. G., Lü, Q. T., Zhou, T. F., Du, J. G., Ding, J., Yan, J. Y., & Lu, Z. T. (2020). Three-dimensional P-wave velocity structure modelling of the middle and lower reaches of the Yangtze River metallogenic belt: Crustal architecture and metallogenic implications. *Acta Geologica Sinica*, *94*(6), 1808–1821. https://doi.org/10.1111/1755-6724.14603

Chen, J. F., & Jahn, B. M. (1998). Crustal evolution of southeastern China: Nd and Sr isotopic evidence. *Tectonophysics*, *284*(1–2), 101–133. https://doi.org/10.1016/s0040-1951(97)00186-8

Cox, K. G. (1980). A model for flood basalt volcanism. *Journal of Petrology*, *21*(4), 629–650. https://doi.org/10.1093/petrology/21.4.629

Doin, M. P., & Henry, P. (2001). Subduction initiation and continental crust recycling: The roles of rheology and eclogization. *Tectonophysics*, *342*(1–2), 163–191. https://doi.org/10.1016/s0040-1951(01)00161-5

Dong, S. W., Ma, L. C., Liu, G., Xue, H. M., Shi, W., & Li, J. H. (2011). On dynamics of the metallogenic belt of middle-lower reaches of Yangtze River, eastern China. *Acta Geologica Sinica*, *85*(5), 612–625.

Flóvenz, Ó. G., & Gunnarsson, K. (1991). Seismic crustal structure in Iceland and surrounding area. *Tectonophysics*, *189*(1–4), 1–17. https://doi.org/10.1016/0040-1951(91)90483-9

Furlong, K. P., & Fountain, D. M. (1986). Continental crustal underplating—Thermal considerations and seismic-petrologic consequences. *Journal of Geophysical Research*, *91*(B8), 8285–8294. https://doi.org/10.1029/jb091ib08p08285

Gao, S., Zhang, B. R., Jin, Z. M., & Hartmut, K. (1999). Lower crustal delamination in the Qinling-Dabie orogenic belt. *Science in China (Series D)*, *42*(4), 423–433.

Goes, S., Govers, R., & Vacher, P. (2000). Shallow mantle temperatures under Europe from P and S wave tomography. *Journal of Geophysical Research*, *105*(B5), 11153–11169. https://doi.org/10.1029/1999jb900300

Griffin, W. L., Begg, G. C., & O'Reilly, S. Z. (2013). Continental-root control on the genesis of magmatic ore deposits. *Nature Geoscience*, *6*(11), 905–910. https://doi.org/10.1038/NGEO1954

Guo, Z., Chen, Y., Ning, J. Y., Yang, Y. J., Afonso, J. C., & Tang, Y. C. (2016). Seismic evidence of on-going sublithosphere upper mantle convection for intra-plate volcanism in Northeast China. *Earth and Planetary Science Letters*, *433*, 31–43. https://doi.org/10.1016/j.epsl.2015.09.035

Hawkesworth, C., Cawood, P., & Dhuime, B. (2013). Continental growth and the crustal record. *Tectonophysics*, *609*, 651–660. https://doi.org/10.1016/j.tecto.2013.08.013

Hedenquist, J. W., & Lowenstern, J. B. (1994). The role of magmas in the formation of hydrothermal ore deposits. *Nature*, *370*(6490), 519–527. https://doi.org/10.1038/370519a0

Hildreth, W., & Moorbath, S. (1988). Crustal contributions to arc magmatism in the Andes of Central Chile. *Contributions to Mineralogy and Petrology*, *98*(4), 455–489. https://doi.org/10.1007/bf00372365

Hou, Z. Q., Zhou, Y., Wang, R., Zheng, Y. C., He, W. Y., Zhao, M., et al. (2017). Recycling of metal-fertilized lower continental crust: Origin of non-arc Au-rich porphyry deposits at cratonic edges. *Geology*, *45*(6), 563–566. https://doi.org/10.1130/G38619.1

Hsü, K. J. (1979). Thin-skinned plate tectonics during Neoalpine orogenesis. *American Journal of Science*, *279*(4), 353–366. https://doi.org/10.2475/ajs.279.4.353

Hu, F. Y., Liu, S. W., Ducea, M. N., Chapman, J. B., Wu, F. Y., & Kusky, T. (2020). Early Mesozoic magmatism and tectonic evolution of the Qinling Orogen: Implications for oblique continental collision. *Gondwana Research*, *88*, 296–332. https://doi.org/10.1016/j.gr.2020.07.006

Jackson, I., & Rigden, S. M. (1998). Composition and temperature of the Earth's mantle: Seismological models interpreted through experimental studies of Earth materials. In I. Jackson (Ed.), *The Earth's mantle: Composition, structure and evolution* (pp. 405–460). Cambridge University Press.

Jiang, G. M., Zhang, G. B., Lü, Q. T., Shi, D. N., & Xu, Y. (2014). Deep geodynamics of mineralization beneath the middle-lower Yangtze River: Evidence from teleseismic tomography. *Acta Petrologica Sinica*, *30*(4), 907–917. (in Chinese with English abstract).

Jones, T. D., & Nur, A. (1984). The nature of seismic reflections from deep crustal fault zones. *Journal of Geophysical Research*, *89*(B5), 3153–3171. https://doi.org/10.1029/jb089ib05p03153

Kay, R. W., & Kay, S. M. (1993). Delamination and delamination magmatism. *Tectonophysics*, *219*(1–3), 177–189. https://doi.org/10.1016/0040-1951(93)90295-u

Lapierre, H., Jahn, B. M., Charvet, J., & Yu, Y. W. (1997). Mesozoic felsic arc magmatism and continental olivine tholeiites in Zhejiang Province and their relationship with the tectonic activity in southeastern China. *Tectonophysics*, *274*(4), 321–338. https://doi.org/10.1016/s0040-1951(97)00009-7

Levshin, A. L., & Ritzwoller, M. H. (2001). Automated detection, extraction, and measurement of regional surface waves. *Pure and Applied Geophysics*, *158*(8), 1531–1545. https://doi.org/10.1007/pl00001233

Li, H. Y., Song, X. D., Lü, Q. T., Yang, X. Y., Deng, Y. F., Ouyang, L. B., et al. (2018). Seismic imaging of lithosphere structure and upper mantle deformation beneath East-central China and their tectonic implications. *Journal of Geophysical Research: Solid Earth*, *123*(4), 2856–2870. https://doi.org/10.1002/2017JB014992

Li, T. Z., Zhao, L., Wan, B., Li, Z. X., Bodin, T., Wang, K., & Yuan, H. Y. (2020). New crustal Vs model along an array in South-East China: Seismic characters and paleo-Tethys continental amalgamation. *Geochemistry, Geophysics, Geosystems*, *21*(7), e2020GC009024. https://doi.org/10.1029/2020GC009024

Li, Z. X. (1994). Collision between the North and South China blocks: A crustal detachment model for suturing in the region east of the tan-Lu fault. *Geology*, *22*(8), 739–742. https://doi.org/10.1130/0091-7613(1994)022<0739:cbtnas>2.3.co;2

Li, Z. X., & Li, X. H. (2007). Formation of the 1300 km-wide intra-continental orogen and post-orogenic magmatic province in Mesozoic South China: A flat-slab subduction model. *Geology*, *35*(2), 179–182. https://doi.org/10.1130/g23193a.1

Lü, Q. T., Meng, G. X., Zhang, K., Liu, Z. D., Yan, J. Y., Shi, D. N., et al. (2021). The lithospheric architecture of the lower Yangtze metallogenic belt, East China: Insights into an extensive Fe-Cu mineral system. *Ore Geology Reviews*, *132*, 103989. https://doi.org/10.1016/j.oregeorev.2021.103989

Lü, Q. T., Shi, D. N., Liu, Z. D., Zhang, Y. Q., Dong, S. W., & Zhao, J. H. (2015). Crustal structure and geodynamics of the Middle and Lower reaches of Yangtze metallogenic belt and neighboring areas: Insights from deep seismic reflection profiling. *Journal of Asian Earth Sciences*, *114*, 704–716. https://doi.org/10.1016/j.jseases.2015.03.022

Lü, Q. T., Yan, J. Y., Shi, D. N., Dong, S. W., Tang, J. T., Wu, M. A., & Chang, Y. F. (2013). Reflection seismic imaging of the Lujiang-Zongyang volcanic basin, Yangtze Metallogenic Belt: An insight into the crustal structure and geodynamics of an ore district. *Tectonophysics*, *606*, 60–77. https://doi.org/10.1016/j.tecto.2013.04.006

Luo, S., Yao, H. J., Li, Q., Wang, W., Wan, K., Meng, Y., & Liu, B. (2019). High-resolution 3D crustal S-wave velocity structure of the Middle-Lower Yangtze River Metallogenic Belt and implications for its deep geodynamic setting. *Science China Earth Sciences*, *62*(9), 1361–1378. https://doi.org/10.1007/s11430-018-9352-9

Luo, Y. H., Yang, Y. J., Xu, Y. X., Xu, H. R., Zhao, K. F., & Wang, K. (2015). On the limitations of interstation distances in ambient noise tomography. *Geophysical Journal International*, *201*(2), 652–661. https://doi.org/10.1093/gji/ggv043

Masters, G., Barmine, M. P., & Kientz, S. (2007). Mineos user's manual. In *Computational infrastructure for geodynamics*. California Institute of Technology.

Mattauer, M., Matte, P., Malavieille, J., Tapponnier, P., Maluski, H., Xu, Z. Q., et al. (1985). Tectonics of the Qinling belt: Build-up and evolution of eastern Asia. *Nature*, *317*(10), 496–500. https://doi.org/10.1038/317496a0

McCuaig, T. C., Beresford, S., & Hronsky, J. (2010). Translating the mineral systems approach into an effective exploration targeting system. *Ore Geology Reviews*, *38*(3), 128–138. https://doi.org/10.1016/j.oregeorev.2010.05.008

Meissner, R. (1989). Rupture, creep, lamellae and crocodiles: Happenings in the continental crust. *Terra Review*, *1*(1), 17–28. https://doi.org/10.1111/j.1365-3121.1989.tb00321.x

Ouyang, L. B., Li, H. Y., Lü, Q. T., Yang, Y. J., Li, X. F., Jiang, G. M., et al. (2014). Crustal and uppermost mantle velocity structure and its relationship with the formation of ore districts in the Middle-Lower Yangtze river region. *Earth and Planetary Science Letters*, *408*, 378–389. https://doi.org/10.1016/j.epsl.2014.10.017

Oxburgh, E. R. (1972). Flake tectonics and continental collision. *Nature*, *239*(22), 202–204. https://doi.org/10.1038/239202a0

Plank, T., Kelley, K. A., Zimmer, M. M., Hauri, E. H., & Wallace, P. J. (2013). Why do mafic arc magmas contain ~4 wt% water on average? *Earth and Planetary Science Letters*, *364*, 168–179. https://doi.org/10.1016/j.epsl.2012.11.044

Price, R. A. (1986). The southeastern Canadian Cordillera: Thrust faults, tectonic wedging, and delamination of the lithosphere. *Journal of Structural Geology*, *8*(3–4), 239–254. https://doi.org/10.1016/0191-8141(86)90046-5

Rawlinson, N., & Sambridge, M. (2005). The fast marching method: An effective tool for tomographic imaging and tracking multiple phases in complex layered media. *Exploration Geophysics*, *36*(4), 341–350. https://doi.org/10.1071/EG05341

Richards, J. P. (2003). Tectono-magmatic precursors for porphyry Cu-(Mo-Au) deposit formation. *Economic Geology*, *98*(8), 1515–1533. https://doi.org/10.2113/gsecongeo.98.8.1515

Rudnick, R. L., & Fountain, D. M. (1995). Nature and composition of the continental crust: A lower crustal perspective. *Reviews of Geophysics*, *33*(3), 267–309. https://doi.org/10.1029/95rg01302

Shen, W. S., Ritzwoller, M. H., Kang, D., Kim, Y. H., Lin, F. C., Ning, J., et al. (2016). A seismic reference model for the crust and uppermost mantle beneath China from surface wave dispersion. *Geophysical Journal International*, *206*(2), 954–979. https://doi.org/10.1093/gji/ggw175

Shi, D. N., Lü, Q. T., Xu, W. Y., Yan, J. Y., Zhao, J. H., Dong, S. W., et al. (2013). Crustal structure beneath the middle-lower Yangtze metallogenic belt in East China: Constraints from passive source seismic experiment on the Mesozoic intra-continental mineralization. *Tectonophysics*, *606*, 48–59. https://doi.org/10.1016/j.tecto.2013.01.012

Sun, W. D., Xie, Z., Chen, J. F., Zhang, X., Chai, Z. F., Du, A. D., et al. (2003). Os-Os dating of copper and molybdenum deposits along the middle and lower reaches of the Yangtze River, China. *Economic Geology*, *98*(1), 175–180. https://doi.org/10.2113/98.1.175

Thybo, H., & Artemieva, I. M. (2013). Moho and magmatic underplating in continental lithosphere. *Tectonophysics*, *609*, 605–619. https://doi.org/10.1016/j.tecto.2013.05.032

Vigneresse, J. L. (1995). Crustal regime of deformation and ascent of granitic magma. *Tectonophysics*, *249*(3–4), 187–202. https://doi.org/10.1016/0040-1951(95)00005-8

Wang, Q., Wyman, D. A., Xu, J. F., Zhao, Z. H., Jian, P., Xiong, X. L., et al. (2006). Petrogenesis of Cretaceous adakitic and shoshonitic igneous rocks in the Luzong area, Anhui province (eastern China): Implications for geodynamics and Cu-Au mineralization. *Lithos*, *89*(3–4), 424–446. https://doi.org/10.1016/j.lithos.2005.12.010

Wu, F. Y., Sun, D. Y., Zhang, G. L., & Ren, X. W. (2000). Deep geodynamics of Yanshan movement. *Geological Journal of China Universities*, *6*, 379–388. (in Chinese with English abstract).

Wyborn, L. A. I., Heinrich, C. A., & Laques, A. L. (1994). Australian Proterozoic mineral systems: Essential ingredients and mappable criteria. *AusIMM Annual Conference*, 109–115.

Xu, J. F., Shinjo, R., Defant, M. J., Wang, Q., & Rapp, R. P. (2002). Origin of Mesozoic adakitic intrusive rocks in the Ningzhen area of east China: Partial melting of delaminated lower continental crust? *Geology*, *30*(12), 1111–1114. https://doi.org/10.1130/0091-7613(2002)030<1111:oomair>2.0.co;2

Xu, T., Zhang, Z. J., Tian, X. B., Liu, B. F., Bai, Z. M., Lü, Q. T., & Teng, J. W. (2014). Crustal structure beneath the Middle-Lower Yangtze metallogenic belt and its surrounding areas: Constraints from active source seismic experiment along the Lixin to Yixing profile in East China. *Acta Petrologica Sinica*, *30*(4), 918–930. (in Chinese with English abstract).

Xu, Y., Lü, Q. T., Zhang, G. B., Jiang, G. M., Zhang, C. R., Shan, X. P., & Wu, Q. (2015). S-wave velocity structure beneath the Middle-Lower Yangtze river metallogenic belt and the constraints on the deep dynamic processes. *Chinese Journal of Geophysics*, *58*(12), 4373–4387. https://doi.org/10.6038/cjg20151204

Xue, H. M., Ma, F., & Cao, G. Y. (2015). Geochronology and petrogenesis of shoshonitic igneous rocks, Luzong volcanic basin, middle and lower Yangtze River reaches, China. *Journal of Asian Earth Sciences*, *110*, 123–140. https://doi.org/10.1016/j.jseaes.2015.03.020

Yan, J. Y., Lü, Q. T., Luo, F., Cheng, S. B., Zhang, K., Zhang, Y. Q., et al. (2021). A gravity and magnetic study of lithospheric architecture and structures of South China with implications for the distribution of plutons and mineral systems of the main metallogenic belts. *Journal of Asian Earth Sciences*, *221*, 104938. https://doi.org/10.1016/j.jseaes.2021.104938

Yang, X. Y., Li, Y. H., Afonso, J. C., Yang, Y. J., & Zhang, A. Q. (2021). Thermochemical state of the upper mantle beneath South China from multi-observable probabilistic inversion. *Journal of Geophysical Research: Solid Earth*, *126*(5), e2020JB021114. https://doi.org/10.1029/2020JB021114

Yang, Y. J., Li, A. B., & Ritzwoller, M. H. (2008). Crustal and uppermost mantle structure in southern Africa revealed from ambient noise and teleseismic tomography. *Geophysical Journal International*, *174*(1), 235–248. https://doi.org/10.1111/j.1365-246x.2008.03779.x

Yang, Y. J., Ritzwoller, M. H., Levshin, A. L., & Shapiro, N. M. (2007). Ambient noise wave tomography across Europe. *Geophysical Journal International*, *168*(1), 259–274. https://doi.org/10.1111/j.1365-246x.2006.03203.x

Yao, H. J., Van der Hilst, R. D., & De Hoop, M. V. (2006). Surface-wave array tomography in SE Tibet from ambient seismic noise and two-station analysis: I—Phase velocity maps. *Geophysical Journal International*, *166*(2), 732–744. https://doi.org/10.1111/j.1365-246x.2006.03028.x

Yin, A., & Nie, S. Y. (1993). An indentation model for the north and south China collision and the development of the Tan-Lu and Honam fault systems, eastern Asia. *Tectonics*, *12*(4), 801–813. https://doi.org/10.1029/93tc00313

Zhang, A., Guo, Z., Afonso, J. C., Yang, Y., Yang, B., & Xu, Y. (2020). The deep thermochemical structure of the Dabie orogenic belt from multi-observable probabilistic inversion. *Tectonophysics*, *787*, 228478. https://doi.org/10.1016/j.tecto.2020.228478

Zhang, Y. Q., Lü, Q. T., Shi, D. N., Yang, Y. J., Afonso, J. C., Xu, Y., et al. (2023). The crustal and uppermost mantle Vs structure of the middle and lower reaches of the Yangtze River metallogenic belt: Implications for metallogenic process [Dataset]. Figshare. https://doi.org/10.6084/m9.figshare.22297906.v1

Zhang, Y. Q., Lü, Q. T., Teng, J. W., Wang, Q. S., & Xu, T. (2014). Discussion on the crustal density structure and deep mineralization background in the Middle-Lower Yangtze metallogenic belt and its surrounding areas: Constraints from the gravity inversion. *Acta Petrologica Sinica*, *30*(4), 931–940. (in Chinese with English abstract).

Zhang, Y. Q., Shi, D. N., Lü, Q. T., Xu, Y., Xu, Z. W., Yan, J. Y., et al. (2021). The crustal thickness and composition in the eastern South China Block constrained by receiver functions: Implications for the geological setting and metallogenesis. *Ore Geology Reviews*, *130*, 103988. https://doi.org/10.1016/j.oregeorev.2021.103988

Zhou, T. F., Fan, Y., & Yuan, F. (2008). Advances on petrogensis and metallogeny study of the mineralization belt of the middle and lower reaches of the Yangtze River area. *Acta Petrologica Sinica*, *24*(8), 1665–1678. (in Chinese with English abstract).